LLNL-JRNL-754342

Observation of excited states in 20Mg sheds light on nuclear forces and shell evolution

J. S. Randhawa, R. Kanungo, M. Holl, J. D. Holt, P. Navratil, S. R. Stroberg, G. Hagen, G. R. Jansen, M. Alcorta, C. Andreoiu, C. Barnes, C. Burbadge, D. Burke, A. A. Chen, A. Chester, G. Christian, S. Cruz, B. Davids, J. Even, G. Hackman, J. Henderson, S. Ishimoto, P. Jassal, S. Kaur, M. Keefe, D. Kisliuk, R. Kruecken, J. Liang, J. Lighthall, E. McGee, J. Measures, M. Moukaddam, E. Padilla-Rodal, A. Shotter, I. J. Thompson, J. Turko, M. Williams, O. Workman

July 6, 2018

Physical Review C

Observation of excited states in ^{20}Mg sheds light on nuclear forces and shell evolution

J.S. Randhawa[1,2], R. Kanungo[1,2], M. Holl[1,2], J. D. Holt[2], P. Navratil[2], S. R. Stroberg[2], G. Hagen[3,4*], G. R. Jansen[5,3*], M. Alcorta[2], C. Andreoiu[6], C. Barnes[1], C. Burbadge[7], D. Burke[8], A. A. Chen[8], A. Chester[6], G. Christian[2], S. Cruz[2], B. Davids[2,9], J.Even[2†], G. Hackman[2], J. Henderson[2], S. Ishimoto[10], P. Jassal[1,2], S. Kaur[1,11], M. Keefe[1], D. Kisliuk[7], R. Krücken[2,12], J. Liang[8], J. Lighthall[2], E. McGee[7], J. Measures[2], M. Moukaddam[2], E. Padilla-Rodal[13], A. Shotter[14], I.J. Thompson[15], J. Turko[7], M.Williams[2,16], O. Workman[1]

[1]*Astronomy and Physics Department, Saint Mary's University, Halifax, NS B3H 3C3, Canada*
[2]*TRIUMF, Vancouver, BC V6T2A3, Canada*
[3]*Physics Division, Oak Ridge National Laboratory, Oak Ridge, Tennessee 37831, USA*
[4] *Department of Physics and Astronomy, University of Tennessee, Knoxville, TN 37996, USA*
[5] *National Center for Computational Sciences, Oak Ridge National Laboratory, Oak Ridge, Tennessee 37831, USA*
[6]*Department of Chemistry, Simon Fraser University, Burnaby, BC V5A 1S6, Canada*
[7]*Department of Physics, University of Guelph, Guelph, ON N1G 2W1, Canada*
[8]*Department of Physics and Astronomy, McMaster University, Hamilton, ON L8S 4M1, Canada*
[9]*Department of Physics, Simon Fraser University, Burnaby, BC V5A 1S6, Canada*
[10]*High Energy Accelerator Research Organization (KEK), Ibaraki 305-0801, Japan*
[11]*Department of Physics and Atmospheric Science, Dalhousie University, Halifax, NS B3H 4R2, Canada*
[12]*Department of Physics and Astronomy, University of British Columbia, Vancouver, BC V6T 1Z1, Canada*
[13]*Instituto de Ciencias Nucleares, UNAM, AP 70-543, 04510 Mexico City, Mexico*
[14]*University of Edinburgh, Edinburgh, United Kingdom*
[15]*Lawrence Livermore National Laboratory, L-414, Livermore, California 94551, USA and*
[16]*Department of Physics, University of York, Heslington, York, United Kingdom, YO10 5DD*

(Dated: November 4, 2018)

The exotic Borromean nucleus ^{20}Mg with $N = 8$, located at the proton drip-line provides a unique testing ground for nuclear forces and the evolution of shell structure in the neutron-deficient region. We report on the first observation of proton unbound resonances together with bound states in ^{20}Mg from the ^{20}Mg(d,d') reaction performed at TRIUMF. Phenomenological shell-model calculations offer a reasonable description. However, our experimental results present a challenge for current first-principles nuclear structure approaches and point to the need for improved chiral forces and *ab initio* calculations. Furthermore, the differential cross section of the first excited state is compared with distorted-wave Born approximation calculations to deduce a neutron quadrupole deformation parameter of β_n=0.46±0.21. This provides the first indication of a possible weakening of the $N = 8$ shell closure at the proton drip-line.

PACS numbers: 24.50+g, 25.45.De, 25.60.-t, 25.70.Ef

The evolution of shell structure over the nuclear landscape is a manifestation of strong interactions in the complex nuclear many-body system. Properties of nuclei at the neutron and proton drip-lines provide new arenas to investigate the effects of large proton-neutron asymmetry and understand the persistence of mirror symmetry. Shell structure evolution in neutron-rich and proton-rich nuclei [1–12] are leading to new insights into nuclear forces, including the role of three-body forces [13, 14]. The region around the $N = 8$ shell closure draws particular interest, since this shell gap disappears at the neutron drip-line and leads to the formation of a two-neutron halo in the Borromean nucleus ^{11}Li. The small two-neutron separation energy ($S_{2n} = 360$ keV) of ^{11}Li results in the excited states of ^{11}Li being unbound. Less is known about the structure of nuclei at the proton drip-line. The $N = 8$ isotone at the proton drip-line, ^{20}Mg, is also a Borromean system whose two-proton separation energy is $S_{2p} = 2.337(27)$ MeV [15]. There is no experimental information on resonances above the proton threshold in ^{20}Mg. In this work we present the first observation of a resonance in ^{20}Mg through deuteron inelastic scattering. This measurement provides new insight into shell evolution as well as tests of *ab initio* predictions. The resonance(s) in ^{20}Mg could also contribute to a potential breakout path from the hot CNO cycle via two-proton capture on the waiting point nucleus ^{18}Ne in Type-I x-ray bursts [16].

*This manuscript has been authored by UT-Battelle, LLC under Contract No. DE-AC05-00OR22725 with the U.S. Department of Energy. The United States Government retains and the publisher, by accepting the article for publication, acknowledges that the United States Government retains a non-exclusive, paidup, irrevocable, world-wide license to publish or reproduce the published form of this manuscript, or allow others to do so, for United States Government purposes. The Department of Energy will provide public access to these results of federally sponsored research in accordance with the DOE Public Access Plan. (http://energy.gov/downloads/doe-public-access-plan)

†Present address: KVI-CART, University of Groningen, 9747 AA Groningen, The Netherlands

Microscopic cluster model [17] calculations predict a 2^+ state that is in fair agreement with that observed [18, 19] around 1.6 MeV, and a 4^+ state is predicted 1 MeV above it, for which no experimental information exists. The 4^+ state is predicted slightly higher, around 3.8 MeV, using a beyond the mean field approach with the Gogny interaction [20]. On the other hand, predictions based on an angular momentum projected generator coordinate framework with the Gogny D1S interaction [21], find the 2_1^+ and the 4_1^+ states to be higher in energy around, 3.5 MeV and 7.8 MeV, respectively. *Ab initio* calculations in a many-body perturbation theory (MBPT) framework including the three-nucleon (3N) force [22] predicts the first excited state in fair agreement with the cluster model [17] and mean field models [20]. The predictions widely vary however, for states above the proton threshold with the 2_2^+ state placed around 4.2 MeV and a nearly degenerate 4_1^+ state placed just above it. Experimental information on these states, especially above the proton threshold, is therefore necessary for testing the nuclear structure models and nuclear forces including possible isospin-symmetry-breaking effects.

In addition, high-precision mass measurements of ^{20,21}Mg [23] cannot be reconciled with the known isobaric mass multiplet equation for ^{20}Mg from isospin symmetric shell-model Hamiltonians [24] or with that including isospin non-conserving interactions [25]. The *ab initio* predictions based on MBPT [22] show a stronger isospin dependence of the IMME than is experimentally observed [23]. On the other hand, the energy of the lowest T = 2, $J^\pi = 0^+$ state in ^{20}Na measured from superallowed β^+ decay of ^{20}Mg shows that the $T = 2$, mass 20 multiplet can be successfully described by a quadratic IMME and does not suggest its breakdown [26]. Excited states of the mirror nuclei ^{20}Mg and ^{20}O can provide further insight into the isospin dependence of the nuclear interaction. Such states can also portray the nature of the N = 8 shell closure at the proton drip-line.

The first excited state of ^{20}Mg is a bound state that was observed first through gamma ray detection from the ^{9}Be(^{22}Mg,^{20}Mg+γ)X reaction [18] exhibiting a peak at 1.598(10) MeV. A gamma transition at 1.61(6) MeV was also observed in the Coulomb excitation of ^{20}Mg with a Pb target at 58.4A MeV [19]. Assuming this as the 2^+ state, a B(E2; $0^+ \rightarrow 2^+$) value of 177(32) e^{2}fm^4 was deduced [19], which is in good agreement with predictions in Refs.[21] as well as the cluster model predictions [17]. In order to obtain insight on the deformation of neutrons in this $N = 8$ isotone, inelastic scattering with a hadronic probe is needed together with information derived from Coulomb excitation.

In this article, we report the first study of deuteron inelastic scattering on ^{20}Mg, populating new resonances together with the ground and first excited states in this proton drip-line nucleus. The experiment was carried out using the IRIS reaction spectroscopy facility [28] at TRIUMF. A schematic view of the detector layout is shown in Fig.1. The radioactive beam of ^{20}Mg was produced via fragmentation of a SiC target with 480 MeV protons. The beam was re-accelerated using the ISAC-II superconducting LINAC [29] to 8.5A MeV and then passed through an ionization chamber, filled with isobutane gas at 19.5 Torr at room temperature. The energy loss of the beam, measured in this detector, provided an event by event identification of the ^{20}Mg incident beam and its contaminant ^{20}Na throughout the experiment. Following this, the beam interacted with a thin windowless solid D_2 reaction target built on a 4.5 μm thick Ag foil backing facing upstream of the D_2 layer. The target cell with the foil was cooled to 4 K, before forming solid D_2. The energy of the elastic scattered beam on the Ag foil was measured with and without D_2, providing a continuous measurement of the target thickness during the experiment. These scattered beam particles were detected using a double sided silicon strip detector placed 33 cm downstream of the target, covering laboratory angles 1.9° to 6.1°. The average target thickness was 65 μm, and the value at each instant of time (each data collection run) was used for determining the scattering cross sections. The deuterons scattered out from reactions were detected using annular arrays of 100 μm thick single sided silicon strip detectors followed by a layer of 12 mm thick CsI(Tl) detectors. This detector combination served as an energy-loss (ΔE) and total energy (E) telescope for identifying the p, d, t and He recoils after the target. The CsI(Tl) detectors were calibrated using the elastic and inelastic scattering from a beam of ^{20}Ne. The detector telescope covered scattering angles of θ_{lab} = 30.1° to 56.2°.

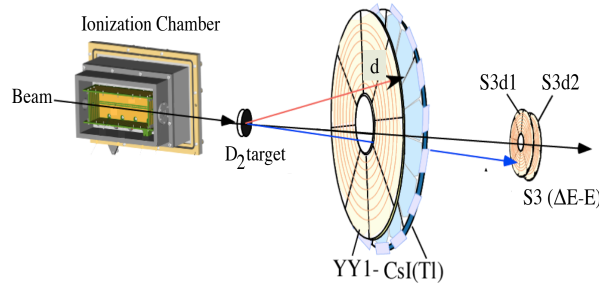

FIG. 1: Schematic view of experimental setup at IRIS

The excitation spectrum of ^{20}Mg, shown in Fig.2a, was reconstructed using the missing mass technique from the energy and scattering angle of the deuterons, measured by the silicon-CsI(Tl) telescope. The deuteron scattering can detect proton unbound resonances with no background from decay protons, unlike proton inelastic scattering. The ground state peak from ^{20}Mg(d,d) elastic scattering is clearly visible together with two prominent peaks, one below and one above the proton threshold. The background from the Ag foil was measured by collecting data without D_2 and is shown with the green dashed-dotted histogram normalized by the inci-

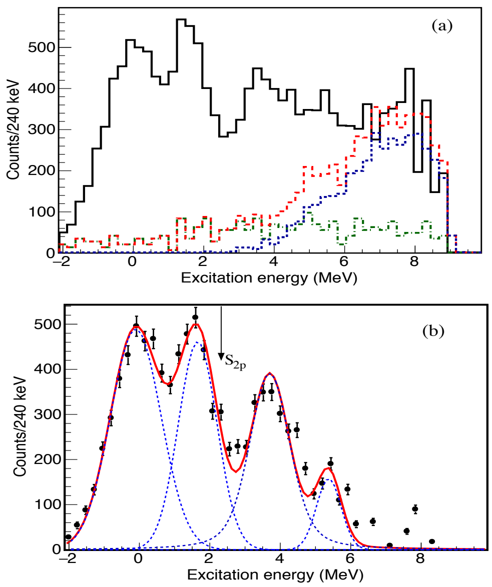

FIG. 2: (a) The excitation energy spectrum for ^{20}Mg measured from ^{20}Mg(d,d') reaction (black histogram). The measured background from Ag backing foil (green dashed-dotted histogram). Background from ^{20}Mg+d $\rightarrow$^{18}Ne+p+p+d four-body phase space (blue dashed histogram). The red histogram shows the total background (sum of blue and green histograms). (b) Background subtracted excitation energy spectrum for ^{20}Mg. The curves show the results of fitting (see text). The blue dashed curves are the individual fitting components and the red curve is the their sum.

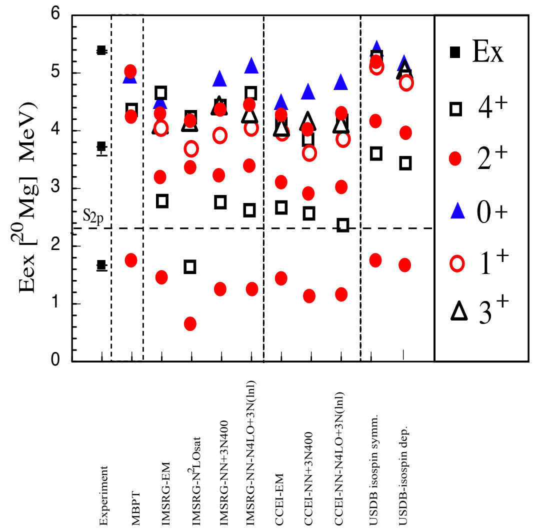

FIG. 3: Measured excited states (this work) in ^{20}Mg (black filled squares) compared to theoretical predictions. *Ab initio* predictions in MBPT framework with the chiral NN+3N interaction [22], IMSRG framework with EM, N^{2}LO$_{\rm sat}$, NN+3N(400) and NN-N^{4}LO+3N(lnl) interactions, CCEI framework with the EM, NN+3N(400) and NN-N^{4}LO+3N(lnl) interactions, and shell model with USDB interactions without and with isospin dependence. The spins of the predicted states are indexed in the figure.

dent beam intensity. This background contribution was $\approx$ 10% of the total spectrum. The non-resonant background from ^{20}Mg+d $\rightarrow$^{18}Ne+p+p+d estimated from Monte Carlo simulation, including the detection conditions, is shown by the blue short dashed histogram. The total background from these two contributions is depicted by the red dashed histogram and is normalized to the data in the excitation energy region greater than 6.5 MeV.

The background subtracted excitation spectrum (Fig.2b), was fitted by a sum of two Gaussians, for the two bound state peaks, and two Breit-Wigner functions folded by Gaussian profiles accounting for the detection resolution, for the unbound resonance peaks. The excitation energy resolution (σ) for the ground state peak was 0.71 MeV for θ_{lab}= 35° and 0.45 MeV for θ_{lab}= 50°, which is in fair agreement with simulations. The resolution improves for the excited states to 0.48 MeV for the newly observed second excited state as determined based on simulations. The excitation energy of the first excited state peak is found to be $1.65^{+0.02}_{-0.10}$ MeV which is in good agreement with the observations in Refs.[18, 19]. Above the proton threshold, the most prominent peak is observed at an excitation energy of $3.70^{+0.02}_{-0.20}$ MeV with an apparent resonance width of 0.47$\pm$0.06 MeV after unfolding the resolution. The excitation energy uncertainties include observable peak shifts for possible systematic effects besides peak fitting. A small structure is also observed at a higher excitation energy of 5.37$\pm$0.02 MeV where the uncertainty quoted is from fitting only.

The energies of the first two excited states states observed in ^{20}Mg are in close agreement with those of the mirror nucleus ^{20}O [27]. Shell model calculations with the phenomenological USDB [24] interaction without any isospin dependence are in fair agreement with the data (see Fig. 3), though the first excited state is predicted slightly higher in energy and the second excited state observed seems closer to the predicted 4^+ state. Calculations with an improved USDB interaction, including the Coulomb corrections and isospin dependence of Ref. [30], provide excellent agreement with the first excited (2^+) state while the observed second excited state is midway between the predicted 4^+_1 and 2^+_2 states. Given the small predicted energy difference of these states, it may be possible that the new resonance peak observed in the experiment is an overlap of these two states. Furthermore, valence-space calculations within the MBPT framework, based on NN+3N forces [22] (within an extended proton valence space that included the sd shell plus $f_{7/2}$ and $p_{3/2}$ orbitals), also predict the first excited 2^+ energy in good agreement with experiment, but higher-lying states are several hundred keV above the observed resonances. This could be expected since these calculations neglect effects of continuum coupling, which typically lower states by a few hundred keV.

New *ab initio* calculations were therefore performed.

In particular, we use the valence-space in medium similarity renormalization group (VS-IMSRG) approach [31–33], and the coupled-cluster effective interaction (CCEI) method [34, 35]. The VS-IMSRG approach constructs an approximate unitary transformation [36, 37] to first decouple the ^{16}O core, as well as an *sd* valence-space Hamiltonian, diagonalized using the NuShellX@MSU shell-model code [38]. We further capture the bulk effects of 3N forces between valence nucleons with the ensemble normal-ordering procedure of Ref. [39], thereby producing a unique valence-space Hamiltonian for each nucleus to be studied. This allows us to test nuclear forces in essentially any fully open-shell system accessible to the nuclear shell model with a level of accuracy comparable to large-space *ab initio* methods. In the CCEI approach, similar to the VS-IMSRG method, one calculates the valence-space effective interaction starting from a chiral NN+3N interaction and applies the obtained zero-plus-one-plus-two-body interaction in the standard shell model diagonalization. The CCEI approach [35] utilizes coupled-cluster method to perform *ab initio* calculations for A_c, $A_c + 1$ and $A_c + 2$ system with A_c the number of nucleons in the core (here $A_c = 16$). The Okubo-Lee-Suzuki similarity transformation [40, 41] is then used to obtain an effective *sd*-shell interaction.

We take several sets of initial NN+3N forces in this work. The first, EM(1.8/2.0) [42, 43], begins from the chiral NN N^{3}LO force [44] with a nonlocal 3N force fit in $A = 3$ and 4-body systems, but reproduces ground- and excited-state energies to the tin region and beyond [45, 46]. The second, NN+3N(400) begins from the same NN force, but with local 3N forces [47, 48], yields accurate binding energies and spectra in and around the oxygen isotopes [32, 34, 49, 50]. Next, we utilized a newly developed chiral potential at N^{4}LO [51] combined with an N^{2}LO 3N interaction with parameters fitted to the ^{3}H binding energy and half-life (NN-N^{4}LO+3N(lnl)). Finally N^{2}LO$_{\rm sat}$ has been fit to medium-mass data and reproduces ground-state energies and radii to the nickel region [52].

VS-IMSRG calculations based on the EM(1.8/2.0) interaction accurately predicts the energy of the first 2^+ state, but states above the proton threshold are lower than the experimental observations as well as the shell model predictions. N^{2}LO$_{\rm sat}$, on the other hand, gives a much too compressed spectrum, with the first excited state at only 600 keV, and ultimately does not produce a reasonable spectrum for ^{20}Mg. The other two interactions, NN+3N400 and NN N^{4}LO+3N(lnl), provide similar results as EM(1.8/2.0), but with slightly lower 2^+_1 energies and a greater spread in higher-lying states. Overall the spacings given by EM(1.8/2.0) are closest to those for the phenomenological USDB, and are consistent with the interpretation of the observed first resonance being comprised of two groups of overlapping states.

While it is difficult to directly compare MBPT with either IMSRG or CCEI since the MBPT results use older generation NN+3N forces and an extended valence space,

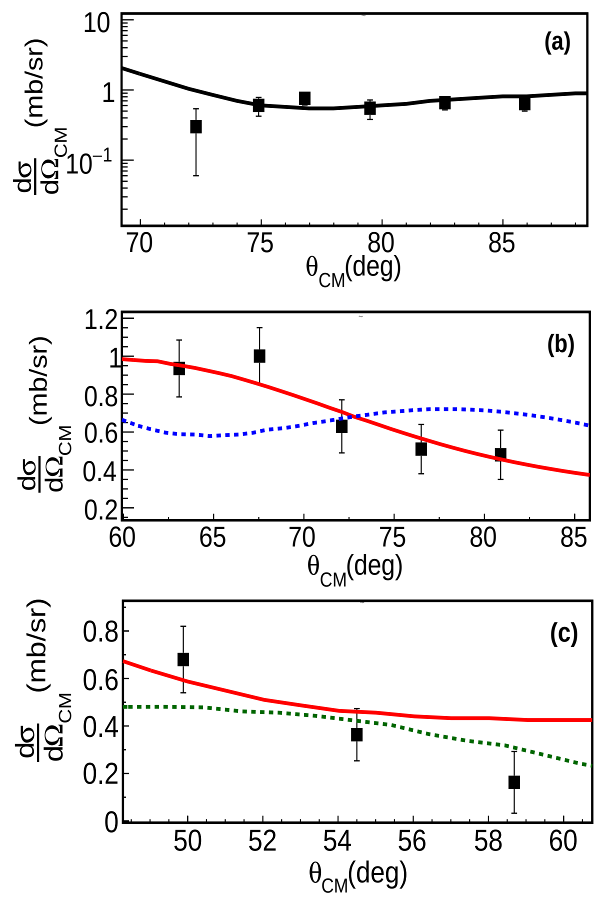

FIG. 4: Angular distribution data (black filled circles) for (a) ^{20}Mg$_{gs}$ (b) ^{20}Mg$_{ex}$; 1.65 MeV (c) b) ^{20}Mg$_{ex}$; 3.7 MeV. The black curve in (a) is a calculation using phenomenological optical model potential. The DWBA calculations are shown by red solid / blue dotted curves for $L = 2$ / $L = 3$ in (b) and red solid/green dotted curve for $L = 2$ / $L = 4$ in (c).

from identical starting interactions, we can evaluate VS-IMSRG and CCEI. We note that very similar results are obtained, with the VS-IMSRG spectrum being modestly more spread. This is likely due to the inclusion of repulsive 3N forces between the four valence protons via the ensemble normal ordering procedure in the VS-IMSRG approach. It appears that there is a much greater variance in the predicted excited states for different prescriptions of the nuclear forces than between the two many-body approaches when one force is considered.

We note that, e.g., the CCEI calculations with NN+3N(400) predict for ^{20}Mg a very reasonable binding energy of 135.2 MeV (compared to the experimental 134.47 MeV) although somewhat compressed excitation spectrum as shown in Fig.3 and discussed above. To further check the VS-IMSRG and CCEI calculations, we also performed no-core shell model (NCSM) [53] calculations with the same interactions. For technical reasons, the largest basis space we could reach was $N_{\rm max} = 6$ (utilizing the importance-truncation approach [54]). Such a space is too small to reach convergence and obtain a reliable estimate of excitation energies. However, our NCSM results within their uncertainties were consistent with the valence-space methods for binding energy as well as for the 2_1^+ state excitation energy. The observed unbound state of ^{20}Mg therefore, points to the need for further refinement of the nuclear forces to reach predictive power at the drip-line. While, the role of continuum effects neglected in all the discussed calculations needs to be assessed it should be noted that coupling to the continuum generally lowers the excitation energy as shown in Ref.[**?**]. Moreover, predictions using the IMSRG framework and the EM interaction (3N-full) in Ref.[33] agree fairly well for Ne and F isotopes. Furthermore, the shell model predictions without any coupling to the continuum agree well with the data.

The differential cross sections of the ground state, first and second excited states were derived from the area under the background subtracted peaks for different angular bins (Fig.4). The Woods-Saxon shape optical potential parameters for the ^{20}Mg+d interaction were determined from the best fit of DWBA calculations to the elastic scattering angular distribution data (Fig.4a) using sFRESCO [56]. These parameters were then used for calculating the angular distributions for the excited state. The angular distribution of the first excited state (Fig.4b) is consistent with a multipolarity of excitation $L = 2$, thereby conclusively determining for the first time its spin of 2^+. The normalization of the calculation to the data provides the deformation length δ where, $\delta = \frac{Z}{A}\delta_p + \frac{N}{A}\delta_n$ with δ_p and δ_n being the proton and neutron deformation lengths, respectively. The deformation length (δ) and deformation parameter (β) are related as $\beta = \delta/R$ with R being the radius. δ_p was determined to be 1.32±0.12 fm from the quadrupole deformation parameter 0.44(4) derived from Coulomb excitation measurements [19] and a proton radius value of 3 fm that is consistent with theoretical predictions [57–59]. The deformation length obtained from ^{20}Mg(d,d') inelastic scattering is $\delta = 1.33\pm0.23$ fm yielding a quadrupole deformation parameter for neutrons, $\beta_n = 0.46\pm0.21$. The large nonzero value within this one standard deviation uncertainty, depicts possible neutron deformation and therefore a first signature of possible weakening of the $N = 8$ shell closure. The β_n for ^{20}Mg is in agreement with $\beta_2 = 0.50(4)$ of the mirror nucleus ^{20}O obtained from proton elastic scattering [60] and also agrees within uncertainties with the proton deformation of ^{20}O, $\beta_{2p} = 0.269(2)$ obtained from B(E2) measurements [61]. The prescription of [60] yields for ^{20}Mg a similar β_n value of 0.46±0.14 and a matrix element ratio of neutrons (M_n) to proton (M_p) of 0.70±0.27.

The angular distribution for the second excited state, shown in Fig.4c, has best fit reduced chi-square values of ≈ 2.7 for $L = 2$ excitation and ≈ 4.1 for $L = 4$ excitation. Therefore, the data are not well explained with either multipolarity. There may be a possibility that the data suggest the resonance peak has a mixture of $L = 2$ and 4. The observed resonance energy is close to the predicted 2_2^+ state with isospin symmetric shell model calculations but lies in between the predicted 2_2^+ and 4^+ states with the isospin dependent USDB interaction. This reflects the importance of isospin dependence effects in the interaction for a better consistency with the observations.

In summary, the first observation of proton unbound excited states in ^{20}Mg at $3.70^{+0.02}_{-0.20}$ MeV and around 5.37 MeV from deuteron inelastic scattering is reported. The data provide sensitive tests of different nuclear forces from chiral effective field theory. New *ab initio* calculations in the VS-IMSRG and CCEI frameworks predict the resonance energies to be lower than observation. Therefore, the new data indicate the challenge in describing nuclei at the proton drip-line with the current chiral forces although ground state binding energies were explained. The results show that some of the different force prescriptions exhibit larger variance in the predicted energy, while the predictions from the two many body methods are similar using the same starting forces. The calculations therefore show some discrimination between the different forces. This work points to the need for improved chiral forces and the *ab initio* methods applied. The spin of the first excited state is determined to be 2^+ and a neutron quadrupole deformation parameter $\beta_n = 0.46\pm0.21$ is found from the differential cross section of this state. The deduced large deformation indicates a possible weakening of the $N = 8$ shell closure at the proton drip-line. The data therefore motivates further theoretical studies with other phenomenological and *ab initio* approaches.

The authors express sincere thanks to the TRIUMF beam delivery team. The support from NSERC, Canada Foundation for Innovation and the Nova Scotia Research and Innovation Trust is gratefully acknowledged. TRIUMF receives funding via a contribution through the National Research Council Canada. The support from RCNP for the target is gratefully acknowledged. It was partly supported by the grant-in-aid program of the Japanese government under the contract number 23224008 and 14J03935. We thank J. Simonis, K. Hebeler, and A. Schwenk for providing the EM interaction 3N matrix elements used in this work and for valuable discussions. Computations were performed with an allocation of computing resources at the Jülich Supercomputing Center (JURECA). This work was performed under the auspices of the U.S. Department of Energy by Lawrence Livermore National Laboratory under Contract DE-AC52-07NA27344. This material is based upon work supported by the U.S. Department of Energy, Office of Science, Office of Nuclear Physics under Award Number DE-SC0018223 (SciDAC-4 NUCLEI) and the Field Work Proposals ERKBP57 and ERKBP72 at Oak Ridge National Laboratory (ORNL). This research used resources of the Oak Ridge Leadership Computing Facility located at ORNL, which is supported by the Office of Science of the Department of Energy under Contract No. DE- AC05-00OR22725. J.E. gratefully acknowledges financial support from the German Academic Exchange Service (DAAD Postdoc program).

[1] R.V.F. Janssens, Nature, **435**, 897 (2005).
[2] R.V.F. Janssens, Nature, **459**, 1069 (2009).
[3] A. Ozawa *et al.*, Phys Rev. Lett. **84**, 5493 (2000).
[4] C.R. Hoffman *et al.*, Phys. Rev. Lett. **100**, 152502 (2008).
[5] R. Kanungo *et al.*, Phys. Rev. Lett. **102**, 152501 (2009).
[6] A. Navin *et al.*, Phys. Rev. Lett. **85**, 266 (2000).
[7] T. Motobayashi *et al.*, Phys. Lett. B **346**, 9 (1995).
[8] B. Bastin *et al.*, Phys Rev. Lett **99**, 022503 (2007).
[9] J.I. Prisciandro *et al.*, Phys. Lett. B **510**, 17 (2001).
[10] F. Wienholtz *et al.*, Nature **498**, 346 (2013).
[11] D. Steppenbeck *et al.*, Nature **502**, 207 (2013).
[12] R. F. Garcia-Ruiz *et al.*, Nature Phys. **12**, 594 (2016).
[13] T. Otsuka *et al.*, Phys. Rev. Lett. **105**, 032501 (2010).
[14] K. Hebeler, J.D. Holt, J. Menéndez, and A. Schwenk, Annu. Rev. Nucl. Part. Sci. **65**, 457 (2015).
[15] M. Wang *et al.*, Chin Phys. **36**, 1603 (2012).
[16] J. Görres *et al.*, Phys. Rev. C **51**, 392 (1995).
[17] P. Descouvemont, Nucl. Phys. A **437**, 7 (1998).
[18] A. Gade *et al.*, Phys. Rev. C **76**, 024317 (2007).
[19] N. Iwasa *et al.*, Phys. Rev. C **78**, 024306 (2008).
[20] T. Rodriguez *et al.* Eur. Phys. Jour A **52**, 190 (2016).
[21] R. Rodriguez-Guzman, J.L. Egido and L.M. Robledo, Nucl. Phys. A **709**, 201 (2002).
[22] J.D. Holt *et al.*, Phys. Rev. Lett. **110**, 022502 (2013).
[23] A.T. Gallant *et al.*, Phys. Rev. Lett. **113**, 082501 (2014).
[24] B.A. Brown *et al.*, Phys. Rev. C **74**, 034315 (2006).
[25] W.E. Ormand *et al.*, Nucl. Phys. A **491**, 1 (1989).
[26] B.E. Glassman *et al.*, Phys. Rev. C **92**, 042501(R) (2015).
[27] S. LaFrance *et al.*, Phys. Rev. C **20**, 1673 (1979).
[28] R. Kanungo, Hyperfine Interactions, **225**, 235 (2014).
[29] R.E. Laxdal *et al.*, Nucl. Instrm. And Meth. B **204**, 400 (2003).
[30] D. W. Hetherington, A. Alousi, and R. B. Moore Nucl. Phys. A **491**, 1 (1989).
[31] K. Tsukiyama *et al.*, Phys. Rev. C **85**, 061304(R) (2012).
[32] S. K. Bogner *et al.*, Phys. Rev. Lett. **113**, 142501 (2014).
[33] S. R. Stroberg *et al.*, Phys. Rev. **C 93**, 051301(R) (2016).
[34] G. R. Jansen, J. Engel, G. Hagen, P. Navratil, and A. Signoracci, Phys. Rev. Lett. **113**, 142502 (2014).
[35] G. R. Jansen, M. D. Schuster, A. Signoracci, G. Hagen, and P. Navratil, Phys. Rev. C **94**, 011301(R) (2016).
[36] T. D. Morris, N. M. Parzuchowski, and S. K. Bogner, Phys. Rev. C **92**, 034331 (2015).
[37] H. Hergert, S. K. Bogner, T. D. Morris, A. Schwenk, and K. Tsukiyama, Phys. Rep. **621**, 165 (2016).
[38] B. A. Brown *et al.*, Nucl. Data Sheets **120**, 115 (2014).
[39] S. R. Stroberg *et al.*, Phys. Rev. Lett. **118**, 032502 (2017).
[40] S. Okubo, Prog. Theor. Phys. **12**, 603 (1954).
[41] K. Suzuki, Prog. Theor. Phys. **68**, 246 (1982).
[42] K. Hebeler *et al.*, Phys. Rev. C **83**, 031301(R) (2011).
[43] J. Simonis *et al.*, Phys. Rev. C **93**, 011302(R) (2016).
[44] D. R. Entem and R. Machleidt, Phys. Rev. C **68**, 041001 (2003).
[45] J. Simonis *et al.*, Phys. Rev. C **96**, 014303 (2017).
[46] T. D. Morris *et al.*, Phys. Rev. Lett. **120**, 152503 (2018).
[47] P. Navratil, Few-Body Syst. **41**, 117 (2007).
[48] R. Roth, S. Binder, K. Vobig, A. Calci, J. Langhammer, and P. Navratil, Phys. Rev. Lett. **109**, 052501 (2012).
[49] H. Hergert, S. Binder, A. Calci, J. Langhammer, and R. Roth, Phys. Rev. Lett. **110**, 242501 (2013).
[50] A. Cipollone, C. Barbieri, and P. Navratil, Phys. Rev. Lett. **111**, 062501 (2013).
[51] D. R. Entem, R. Machleidt, and Y. Nosyk, Phys. Rev. C **96**, 024004 (2017).
[52] A. Ekström *et al.*, Phys. Rev. C **91** (2015).
[53] B. R. Barrett, P. Navratil, and J. P. Vary, Prog. Part. Nucl. Phys. **69**, 131 (2013).
[54] R. Roth and P. Navratil, Phys. Rev. Lett. **99**, 092501 (2007).
[55] G. Hagen *et al.*, Phys. Scripta, **91**, 063006 (2016).
[56] I.J. Thompson, Computer Physics Reports **7**, 167 (1988).
[57] M.K. Gaidarov *et al.*, Phys. Rev. C **89**, 064301 (2014).
[58] Z. Wang and Z. Ren, Nucl. Phys. A **794**, 47 (2007).
[59] G.A. Lalazissis *et al.*, Phys. Rev. C **63**, 034305 (2001).
[60] J.K. Jewell *et al.*, Phys. Lett. **B 454**, 181 (1999).
[61] B. Pritychenko *et al.*, At. Data and Nucl. Data Tables **107**, 1 (2016).